

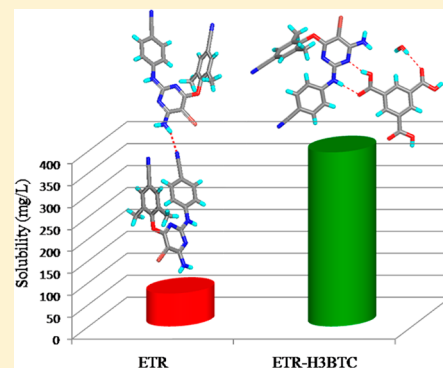
# New Solid Forms of the Anti-HIV Drug Etravirine: Salts, Cocrystals, and Solubility

Lalit Rajput, Palash Sanphui, and Gautam R. Desiraju\*

Solid State and Structural Chemistry Unit, Indian Institute of Science, Bangalore 560 012, India

## Supporting Information

**ABSTRACT:** Thirteen new solid forms of etravirine were realized in the process of polymorph and cocrystal/salt screening to improve the solubility of this anti-HIV drug. One anhydrous form, five salts (hydrochloride, mesylate, sulfate, besylate, and tosylate), two cocrystals (with adipic acid and 1,3,5-benzenetricarboxylic acid), and five solvates (formic acid, acetic acid, acetonitrile, and 2:1 and 1:1 methanolates) were obtained. The conformational flexibility of etravirine suggests that it can adopt four different conformations, and among these, two are sterically favorable. However, in all 13 solid forms, the active pharmaceutical ingredient (API) was found to adopt just one conformation. Due to the poor aqueous solubility of the API, the solubilities of the salts and cocrystals were measured in a 50% ethanol–water mixture at neutral pH. Compared to the salts, the cocrystals were found to be stable and showed an improvement in solubility with time. All the salts were dissociated within an hour, except the tosylate, which showed 50% phase transformation after 1 h of the slurry experiment. A structure property relationship was examined to analyze the solubility behavior of the solid forms.



## INTRODUCTION

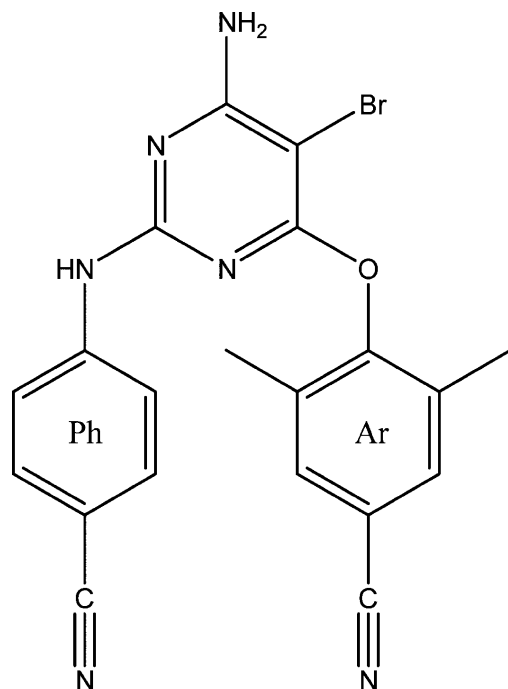
Crystal engineering with the synthon-based approach for the formation of multicomponent molecular crystals of active pharmaceutical ingredients (APIs) has received major attention from chemists because of its fundamental importance and potential for direct applications in the pharmaceutical industry.<sup>1</sup> This approach has shown that major variations in terms of properties of a drug can be achieved by using a GRAS (generally regarded as safe)<sup>2</sup> cofomer, especially in obtaining advantageous stability, solubility, bioavailability, and tableting attributes.<sup>3</sup> Almost 40% of the APIs in the market today face a major problem of poor aqueous solubility.<sup>4</sup> Poor aqueous solubility can be improved by making an amorphous phase through solid dispersion or by using a polymer, additive, excipient, or cyclodextrin.<sup>5</sup> However, salt or cocrystal formation is still one of the best approaches for solubility improvement without disturbing the inherent properties of the API. Cocrystal formation can improve solubility by 4–160 times, whereas salts can modulate solubility 100–1000 fold.<sup>6</sup> Due to their superior solubilities, more than 50% of the APIs are marketed as salts. However, salt formation can sometimes lead to lower stabilities and, hence, low solubility.<sup>7</sup> The physical properties of crystalline solids are a reflection of the molecular arrangement and can be tuned by altering the intermolecular interactions between molecules. For this, structure–property relationship studies are helpful to understand the nature of the multicomponent molecular crystals; this further helps in an understanding of the fundamentals of crystallization and molecular recognition.<sup>8</sup>

In continuation of our efforts to improve the physicochemical properties of APIs with the crystal engineering approach, we have selected an anti-HIV drug, etravirine (ETR).<sup>9</sup> Etravirine, 4-[[[6-amino-5-bromo-2-[(4-cyanophenyl)-amino]-4-pyrimidinyl]oxy]-3,5-dimethylbenzimidazole], is a non-nucleoside reverse transcriptase inhibitor (NNRTI), which binds to HIV-1 reverse transcriptase and blocks the DNA polymerase activities by disrupting the enzyme's catalytic site.<sup>10</sup> It is believed that it binds in at least two conformationally distinct modes, due to its flexibility. There is a report on the polymorph screening (forms A to M) of etravirine characterized by PXRD, DSC, and solid-state NMR.<sup>10c</sup> Further, a cocrystal of etravirine–nicotinamide characterized by PXRD is reported.<sup>10d</sup> Etravirine (brand name Intelence, formerly known as TMC125, is marketed by Tibotec) is a BCS class IV drug and exhibits low solubility and permeability.<sup>11</sup> It is almost insoluble in water over a wide range of pH and is stable at room temperature nearly indefinitely. It is a flexible molecule which has a central pyrimidine ring with two arm phenyls bridged via an ether linkage (Ar–phenyl) and a secondary amine linkage (Ph–phenyl). Both the phenyl arms have terminal cyano functionality in the para position (Scheme 1). Since the molecule has multiple hydrogen bond donor and acceptor sites, there is a high probability for the formation of cocrystals or salts (Scheme 2). Molecular modeling studies suggest that there is a possibility of polymorphism due to different possible

Received: May 7, 2013

Revised: June 4, 2013

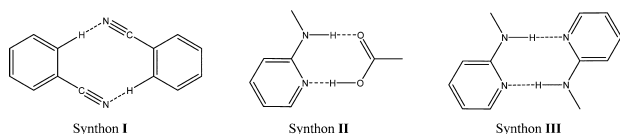
Scheme 1. Schematic Representation of Etravirine and Its New Solid Forms



Etravirine (ETR)

- 1: ETR
- 2: HETR•Cl
- 3: HETR•CH<sub>3</sub>SO<sub>3</sub>
- 4: HETR•HSO<sub>4</sub>•CH<sub>3</sub>OH
- 5: HETR•C<sub>6</sub>H<sub>5</sub>SO<sub>3</sub>
- 6: HETR•MeC<sub>6</sub>H<sub>4</sub>SO<sub>3</sub>
- 7: ETR•ADP (2:1)
- 8: ETR•H<sub>3</sub>BTC•H<sub>2</sub>O
- 9: ETR•HCOOH
- 10: ETR•CH<sub>3</sub>COOH
- 11: ETR•CH<sub>3</sub>OH (2:1)
- 12: ETR•CH<sub>3</sub>OH (1:1)
- 13: ETR•CH<sub>3</sub>CN

Scheme 2. Synthons Observed in the Crystal Structures of Etravirine Solid Forms



conformations of this flexible molecule (Scheme 3). Although extensive studies are in progress on the biological/clinical activity of the drug, it is surprising that there is no report to date on the crystal structure of etravirine or its cocrystals/salts.<sup>12</sup>

It may be useful to comment on some general nomenclature issues pertaining to terms like “salt”, “cocrystal”, “solvates”, and so on because these terms are widely used in the crystal engineering literature. It is not the intention to provide a detailed review here. It may suffice to say that the United States Food and Drug Administration (U.S. FDA) has recently come up with some guidelines for the nomenclature of cocrystals<sup>13</sup> and also that a large group of authors have coauthored a

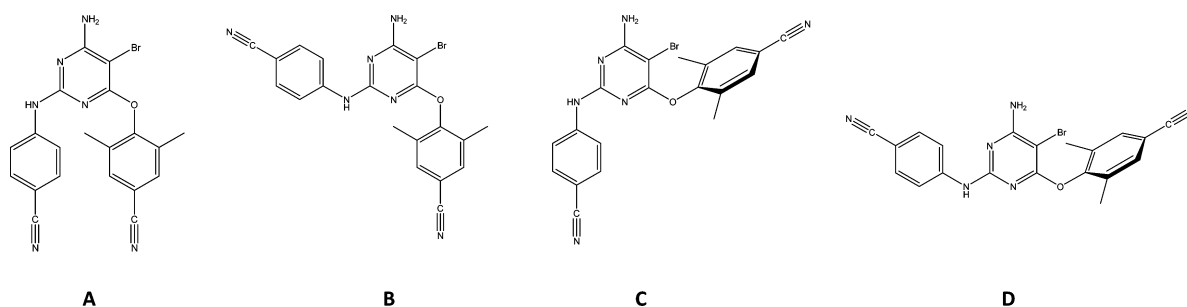
publication suggesting some operational guidelines.<sup>14</sup> The U.S. FDA guidelines state that if the difference in pKa between the proton donor and acceptor is less than 1.0, the substance should be considered as being a cocrystal. If this difference is greater than 1.0, the substance is assumed to be a salt, but more spectroscopic confirmation has been deemed necessary.<sup>13</sup> Single crystal X-ray analysis will provide definitive answers in almost all cases. We feel that the so-called “rule of three” is still a fairly reliable measure to judge a compound as a salt or a cocrystal.

In this report, we discuss our efforts to improve the solubility of etravirine by preparing its crystalline salts and cocrystals and by studying their structural aspects and structure–property relationships. The new solid forms are characterized by FT-IR, DSC, powder and single crystal X-ray diffraction.

## RESULTS AND DISCUSSION

Etravirine was screened for new solid phases (single component and multicomponent systems) using high-throughput crystallization. It is observed that due to the imbalance of donor (three) and acceptor (five) sites, the API has a tendency to

Scheme 3. Different Possible Conformations of Etravirine



B

Table 1. Crystallographic Parameters of Compounds 1–13

compound	1	2	3	4	5	6	7
empirical formula	C <sub>20</sub> H <sub>15</sub> N <sub>6</sub> OBr	C <sub>20</sub> H <sub>16</sub> N <sub>6</sub> OClBr	C <sub>21</sub> H <sub>19</sub> N <sub>6</sub> O <sub>4</sub> SBr	C <sub>21</sub> H <sub>20</sub> N <sub>6</sub> O <sub>6</sub> SBr	C <sub>26</sub> H <sub>21</sub> N <sub>6</sub> O <sub>4</sub> SBr	C <sub>27</sub> H <sub>23</sub> N <sub>6</sub> O <sub>4</sub> SBr	C <sub>23</sub> H <sub>20</sub> N <sub>6</sub> O <sub>3</sub> Br
formula wt	435.29	471.75	531.39	564.40	593.46	607.48	508.35
crystal system	orthorhombic	monoclinic	triclinic	triclinic	monoclinic	monoclinic	triclinic
space group	<i>Pna</i> 2 <sub>1</sub>	<i>P</i> 2 <sub>1</sub> / <i>c</i>	<i>P</i> $\bar{1}$	<i>P</i> $\bar{1}$	<i>P</i> 2 <sub>1</sub>	<i>P</i> 2 <sub>1</sub> / <i>c</i>	<i>P</i> $\bar{1}$
T (K)	150	150	150	150	150	293	150
<i>a</i> (Å)	19.885(5)	8.897(4)	8.225(9)	8.460(16)	8.988(2)	8.769(14)	8.124(1)
<i>b</i> (Å)	10.789(3)	16.622(4)	8.668(10)	8.627(17)	12.801(2)	13.86(2)	11.984(1)
<i>c</i> (Å)	8.712(2)	14.378(6)	15.857(18)	16.65(3)	22.956(8)	22.91(4)	13.515(1)
$\alpha$ (deg)	90	90	88.56(2)	97.44(3)	90	90	64.231(12)
$\beta$ (deg)	90	106.923(16)	87.00(2)	90.58(3)	95.655(15)	97.058(12)	83.606(15)
$\gamma$ (deg)	90	90	88.85 (2)	90.90(3)	90	90	87.777(14)
volume (Å <sup>3</sup> )	1869(8)	2034.1(13)	1131(2)	1205(4)	2628.4(12)	2763(7)	1177.49(13)
<i>D</i> <sub>calcd</sub> (g cm <sup>-3</sup> )	1.547	1.540	1.561	1.556	1.500	1.460	1.434
<i>Z</i>	4	4	2	2	4	4	2
2 $\theta$ range	2.1 to 27.5	2.4 to 27.5	2.3 to 27.5	2.4 to 27.5	1.8 to 27.5	1.8 to 27.5	3.0 to 27.5
<i>R</i> <sub>1</sub> [ <i>I</i> > 2 $\sigma$ ( <i>I</i> )], <i>wR</i> <sub>2</sub>	0.0449, 0.1379	0.0606, 0.1860	0.0468, 0.1352	0.0752, 0.2381	0.0718, 0.2047	0.0911, 0.2196	0.0509, 0.1629
GOF	1.144	1.053	1.038	1.065	1.064	1.334	0.947
diffractometer	Rigaku-CCD	Rigaku-CCD	Rigaku-CCD	Rigaku-CCD	Rigaku-CCD	Rigaku-CCD	Rigaku-CCD
compound	8	9	10	11	12	13	
empirical formula	C <sub>29</sub> H <sub>23</sub> N <sub>6</sub> O <sub>8</sub> Br	C <sub>21</sub> H <sub>17</sub> N <sub>6</sub> O <sub>3</sub> Br	C <sub>22</sub> H <sub>19</sub> N <sub>6</sub> O <sub>3</sub> Br	C <sub>41</sub> H <sub>34</sub> N <sub>12</sub> O <sub>3</sub> Br <sub>2</sub>	C <sub>21</sub> H <sub>19</sub> N <sub>6</sub> O <sub>2</sub> Br	C <sub>42</sub> H <sub>32</sub> N <sub>13</sub> O <sub>2</sub> Br <sub>2</sub>	
formula wt	663.44	481.32	495.34	902.62	467.32	910.63	
crystal system	triclinic	orthorhombic	monoclinic	triclinic	monoclinic	monoclinic	
space group	<i>P</i> $\bar{1}$	<i>Pna</i> 2 <sub>1</sub>	<i>P</i> 2 <sub>1</sub> / <i>n</i>	<i>P</i> $\bar{1}$	<i>P</i> 2 <sub>1</sub> / <i>c</i>	<i>P</i> 2 <sub>1</sub> / <i>n</i>	
T (K)	150	150	150	150	150	150	
<i>a</i> (Å)	8.0836(16)	22.244(5)	8.5277(13)	8.587(9)	16.337(3)	8.6128(2)	
<i>b</i> (Å)	8.9850(15)	10.857(3)	22.639(3)	16.131(15)	13.845(2)	20.9616(7)	
<i>c</i> (Å)	19.589(4)	8.7559(16)	11.345(2)	16.241(15)	20.240(4)	11.2537(4)	
$\alpha$ (deg)	93.209(9)	90	90	64.59(3)	90	90	
$\beta$ (deg)	91.009(12)	90	92.995(9)	82.83(4)	112.841(6)	90.511(2)	
$\gamma$ (deg)	99.211(8)	90	90	80.35(4)	90	90	
volume (Å <sup>3</sup> )	1401.7(4)	2114.6(8)	2187.2(6)	2000(3)	4218.9(13)	2031.64(11)	
<i>D</i> <sub>calcd</sub> (g cm <sup>-3</sup> )	1.572	1.512	1.504	1.499	1.472	1.489	
<i>Z</i>	2	4	4	2	8	2	
2 $\theta$ range	2.1 to 27.5	2.6 to 27.5	2.0 to 27.5	2.4 to 27.5	2.0 to 27.5	2.66 to 26.99	
<i>R</i> <sub>1</sub> [ <i>I</i> > 2 $\sigma$ ( <i>I</i> )], <i>wR</i> <sub>2</sub>	0.0563, 0.1667	0.0529, 0.1525	0.0561, 0.1810	0.0517, 0.1674	0.0564, 0.1632	0.0378, 0.0922	
GOF	1.079	1.088	1.161	1.065	1.128	1.029	
diffractometer	Rigaku-CCD	Rigaku-CCD	Rigaku-CCD	Rigaku-CCD	Rigaku-CCD	Bruker APEX-II CCD	

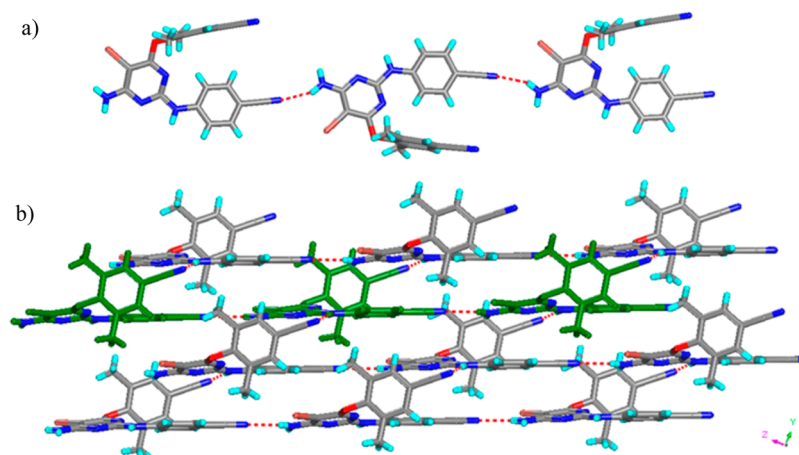


**Figure 1.** Crystal structure of anhydrous form, 1: (a) 1D Chain via N–H···N hydrogen bonds and (b) corrugated 2D layer assembled exclusively via N–H···N hydrogen bonds viewed along the *a*-axis (one of the 1D chains is shown in green).

form solvates/hydrates, while the weak basicity of the API makes it prone to form salts with strong acids. Thirteen new solid forms were obtained from different solvent and solvent

combinations: anhydrous form (1), five salts: hydrochloride (2), mesylate (3), sulfate (4), besylate (5), and tosylate (6), two cocrystals: with adipic acid (ADP) (7) and 1,3,5-

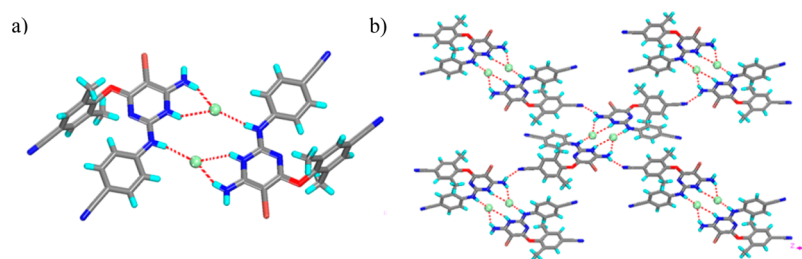


**Figure 2.** Crystal structure of hydrochloride salt, **2**: (a) dimeric unit of protonated etravirine bridged by  $\text{Cl}^-$  ions and (b) the 2D layer involving the dimeric units linked via  $\text{N-H}\cdots\text{N}$  hydrogen bonds.

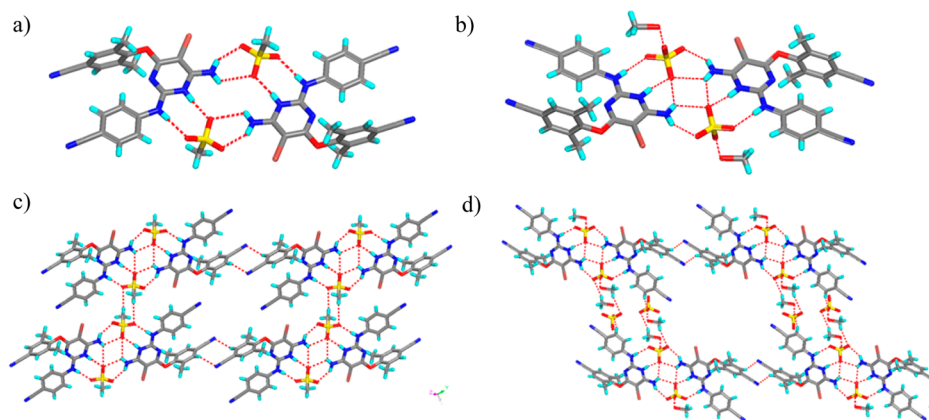


**Figure 3.** Dimeric units of protonated etravirine bridged by corresponding sulfate anions in compound (a) **3** and (b) **4**. 2D layers are present in compounds (c) **3** and (d) **4**. (Notice synthon I and hydrophilic chains).

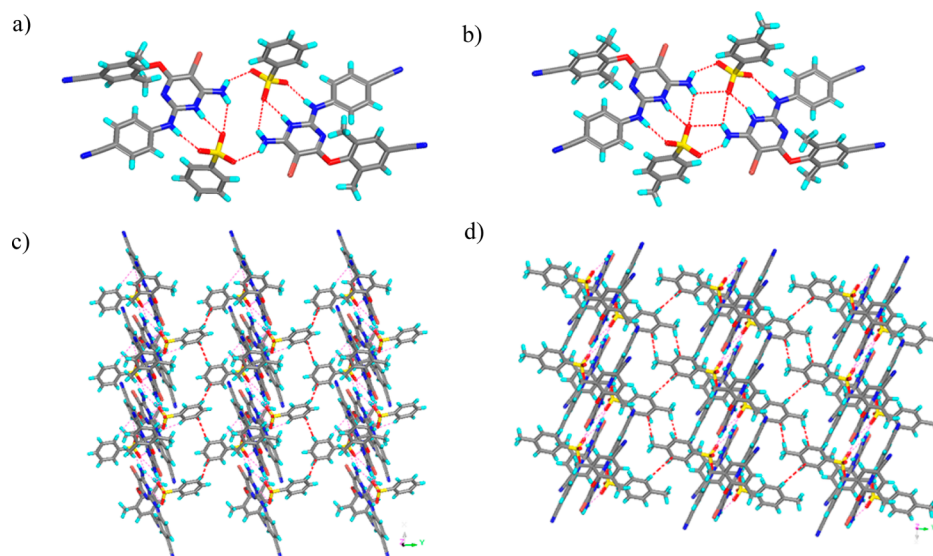


**Figure 4.** Dimeric units of protonated etravirine bridged by corresponding sulfate anions in compound (a) **5** and (b) **6**. 2D layers are present in compounds (c) **5** and (d) **6**. (Notice the sliding of dimeric units as well as hydrophobic interactions).

benzenetricarboxylic acid ( $\text{H}_3\text{BTC}$ ) (**8**) and five solvates: formic acid (**9**), acetic acid (**10**), 2:1 ETR:MeOH (**11**), 1:1 ETR:MeOH (**12**), and acetonitrile (**13**). Despite several cocrystallization attempts with mono- and dicarboxylic acids, we failed to obtain single crystals of cocrystals, except with ADP and  $\text{H}_3\text{BTC}$ . The crystallographic parameters and solubility results are summarized in Tables 1 and 2, respectively. We now discuss the structural aspects of these new multicomponent crystals of etravirine.

**Anhydrous Form (1).** The molecule crystallizes in the orthorhombic crystal system with the  $Pna2_1$  space group ( $Z = 4$ ). The molecule adopts a V-shaped geometry (conformation **A**, Scheme 3), and both the arm phenyls are oriented on the same side of the central pyrimidine ring, as shown in Figure 1a. Within the molecule, the phenyl rings interact with each other via edge-to-face  $\pi\cdots\pi$  interactions with a closest  $\text{C}\cdots\text{C}$  distance of 3.699 Å. The molecule assembles into one-dimensional (1D) chains via  $\text{N-H}\cdots\text{N}$  hydrogen bonds between the primary amine and cyano groups of the Ph-ring. The 1D chain is further

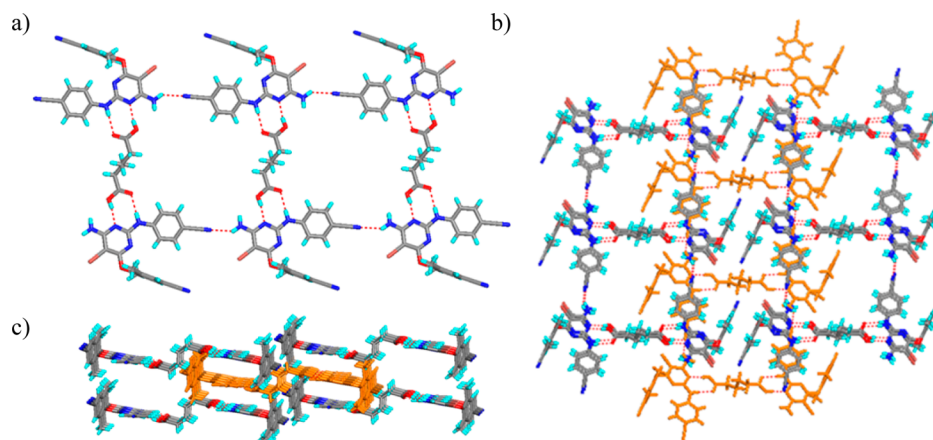


**Figure 5.** Crystal structure of cocrystal 7: (a) synthon II between etravirine and adipic acid forming a ladder network. 3D packing of the ladders (b) top view and (c) side view (one of the ladder is shown in dark yellow).

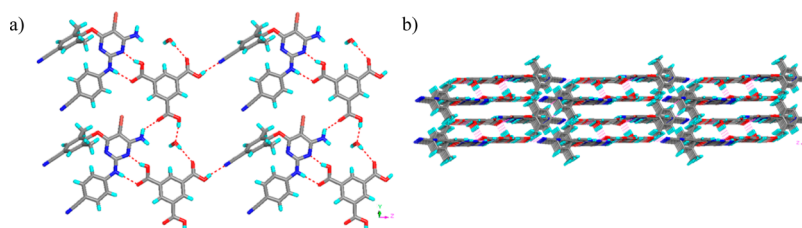


**Figure 6.** Crystal structure of cocrystal 8: (a) synthon II between etravirine and H<sub>3</sub>BTC in a 2D layer and (b) 3D packing of the layers through water bridging and the C–H...N hydrogen bond.

propagated to corrugated two-dimensional (2D) layers via N–H...N hydrogen bonds between the secondary amine and cyano group of the Ar ring (Figure 1b).

**Hydrochloride Salt (2).** The salt crystallizes in the monoclinic crystal system with the  $P2_1/c$  space group ( $Z = 4$ ). Protonated etravirine adopts a V-shaped geometry and two such inversion related molecules form dimeric units bridged by two Cl<sup>−</sup> anions (Figure 2a). The Cl<sup>−</sup> anion is trifurcated in the molecular plane and is hydrogen bonded to the secondary amine NH group of one molecule and the primary amine NH<sub>2</sub> and a protonated pyrimidine NH group of another. Each dimeric unit is hydrogen bonded with four adjacent dimeric units through N–H...N hydrogen bonds, forming a 2D layer (Figure 2b).

**Mesylate (3) and Sulfate (4) Salt.** The mesylate salt (3) crystallizes in the triclinic system with the  $P\bar{1}$  space group ( $Z = 2$ ). Protonated etravirine adopts a V-shaped geometry and two such molecules form dimeric units bridged by two mesylate anions (Figure 3a). In the molecular plane, the mesylate anion is strongly hydrogen bonded to the primary amine NH<sub>2</sub> group of one molecule and the secondary amine NH, protonated pyrimidine NH, and the phenyl CH of another molecule. Each dimeric unit is hydrogen bonded to two adjacent dimeric units via synthon I, forming a 1D chain. The 1D chain is assembled into a 2D layer through dimeric C–H...O hydrogen bonds between the mesylate anions and dimeric weak Br... $\pi$  (closest C...Br distance: 3.54 Å) interactions (Figure 3c). Interestingly, alternate hydrophilic chains of mesylate anions and hydrophobic chain of phenyl rings are present within the 2D layer.

Compound 4 also exhibits similar features as the mesylate salt (Figure 3, panels b and d). To compensate for the methyl group of the mesylate fragment, compound 4 includes a methanol molecule in the unit cell. The crystals of the salt 4 are

not stable at room temperature and rapidly lose crystallinity after exposure to air.

**Besylate (5) and Tosylate (6) Salt.** Both the salts crystallize in the monoclinic system with space group  $P2_1$  for 5 and  $P2_1/c$  for 6. As in the mesylate anion, the besylate and tosylate anions also form the same synthon as shown in Figure 4 (panels a and b). However, the overall packing of 5 and 6 differs significantly from 3 and 4 due to the presence of the bulky phenyl ring compared to the methyl group in the mesylate salt. Along the crystallographic  $a$ -axis, dimer units slide over adjacent units and interact with each other through dipole–dipole interactions, forming a 1D chain. The 1D chain in both the salts is assembled into 2D layers in the  $ab$ -plane via hydrophobic interactions. In 5, the 1D chain is exclusively assembled through edge-to-edge aromatic interactions (closest C...C distances: 3.47 Å and 3.56 Å) between the besylate anions (Figure 4c). However, in 6, it is assembled via edge-to-edge aromatic interactions (closest C...C distances: 3.86 Å) as well as the dimeric C–H... $\pi$  (C...C distance: 3.68 Å) interactions between the tosylate anions (Figure 4d).

**Adipic Acid Cocrystal (7).** The cocrystal 7 crystallizes in triclinic ( $P\bar{1}$ ),  $Z = 2$ . Etravirine adopts a V-shaped geometry and forms synthon II with the acid. The structure is a ladder network where the adipic acid units join the 1D chains of the API (as observed in 1) (Figure 5a). The ladders are packed in an offset fashion. The 1D chains of the ladders involving the API overlap over each other (Figure 5b). In the ladder plane, the adjacent ladders are linked with C–H... $\pi$  interactions between the Ar-ring and the methyl group CH (closest C...C distances: 3.56 Å). The butyl spacer of the adipic acid adopts a *gauche-anti-gauche* conformation which subsequently holds the 1D chains of the API at different planes (Figure 5c). The overall 3D packing of the ladders is in an ABAB manner.

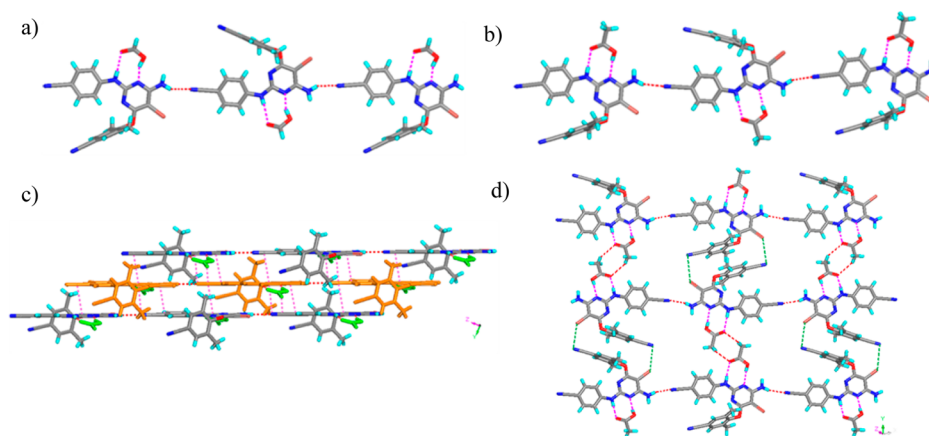


**Figure 7.** 1D chain of molecular complex of the acid-API involving synthon II in (a) **9** and (b) **10**. (c) 2D layer of **9** (dipole-dipole interactions are shown in pink, one of the 1D chain in dark yellow and formic acid molecules in green color). (d) 2D layer of **10**, involving acetic acid hydrogen bonded dimers and halogen bond.

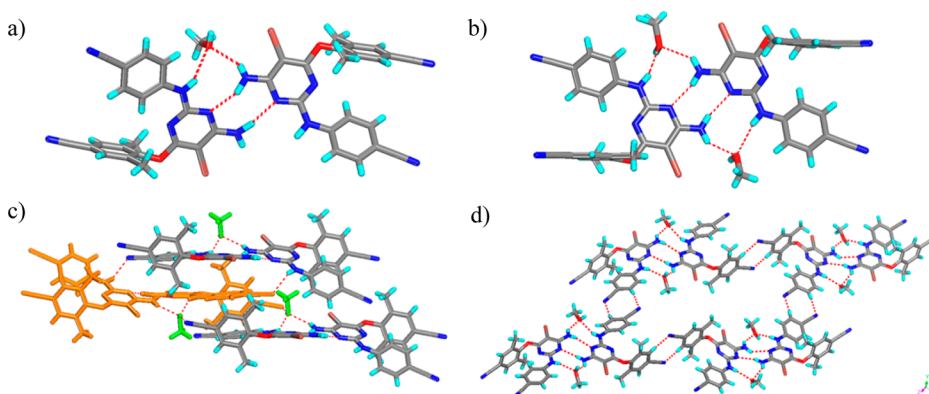


**Figure 8.** Dimeric units involving MeOH molecules in (a) **11** and (b) **12**. (c) Interactions of one of the dimers with the adjacent dimers in **11** (one of the dimers is shown in dark yellow color and MeOH in green) and (d) a 2D layer of **12** involving synthon I.

**Benzenetricarboxylic Acid Cocrystal Hydrate (8).** In the cocrystal **8**, etravirine adopts a V-shaped geometry and forms synthon II with the acid (Figure 6a). The etravirine-acid aggregate forms a 1D chain via strong O–H...N hydrogen bonds between the OH group of the acid and the CN group of the aromatic ring. The 1D chain is further propagated to a 2D layer in the *bc*-plane through N–H...O hydrogen bonds between the primary NH<sub>2</sub> and carbonyl of H<sub>3</sub>BTC, as well as water bridging between two H<sub>3</sub>BTC units. The 2D layer has a planar geometry and is packed in 3D with an ABAB pattern. The AB layers interact with each other via hydrogen bonds involving water molecules, while the BA are held together via C–H...N hydrogen bonds (Figure 6b).

**Formic Acid (9) and Acetic Acid (10) Molecular Complexes.** Compound **9** crystallizes in the orthorhombic crystal system (*Pna*2<sub>1</sub>), while **10** is monoclinic (*P2*<sub>1</sub>/*n*). In both cases, etravirine and the acid form synthon II. The API forms 1D chains via N–H...N hydrogen bonds between the primary amine and the cyano group of the Ph-ring, as observed in **1** (Figure 7, panels a and b). However, the 2D and 3D packing differs significantly from **1**.

The 1D chain of **9** is packed in the *bc*-plane via  $\pi\cdots\pi$  interactions with a closest C...C distance of 3.40 Å and dipole-dipole interactions between the CN group and the pyrimidine C=N bond ( $N_{CN}\cdots C_{PYM}$  distance: 3.31 Å and  $C_{CN}\cdots N_{PYM}$  distance: 3.32 Å) (Figure 7c). However, in **10**, the 1D chain is assembled into a 2D layer in the *ab*-plane with C–H...O

hydrogen bonds between the acetic acid molecules, halogen bonds between Br...N (3.48 Å), and face-to-face  $\pi\cdots\pi$  interactions between the Ar rings (closest C...C distance: 3.50 Å) (Figure 7d).

**Methanol Solvates (11 and 12).** 2:1 (**11**) and 1:1 (**12**) methanolates of the API were obtained concomitantly from MeOH. Compound **11** crystallizes in the triclinic system with a *P* $\bar{1}$  space group and **12** takes the monoclinic *P2*<sub>1</sub>/*c* space group. In both cases, etravirine interacts with each other through synthon III (Figure 8, panels a and b), forming a dimer. This dimer is hydrogen bonded to one MeOH molecule in **11** and symmetrically to two MeOH molecules in **12**.

In **11**, the dimers interact with the adjacent units via N–H...N hydrogen bonds between the cyano group and the primary amine NH<sub>2</sub> and secondary amine NH functionalities forming a corrugated 2D layer in the *ab*-plane (Figure 8c). The dimeric units in **12** are assembled into a 2D layer in the *ac*-plane via synthon I (Figure 8d). The adjacent 2D layers are interdigitated and form a bilayer, involving face-to-face  $\pi\cdots\pi$  (the closest C...C distance of 3.48 Å) interactions between the Ar rings of the layers.

**Acetonitrile Solvate (13).** The acetonitrile solvate of etravirine exhibits the same features as the anhydrous form. They differ only in the 3D packing. For compound **13**, the 2D layers are held together by acetonitrile molecular chains for further 3D packing, which involves C–H...N and C–H...Br hydrogen bonds (Figure S1 of the Supporting Information).

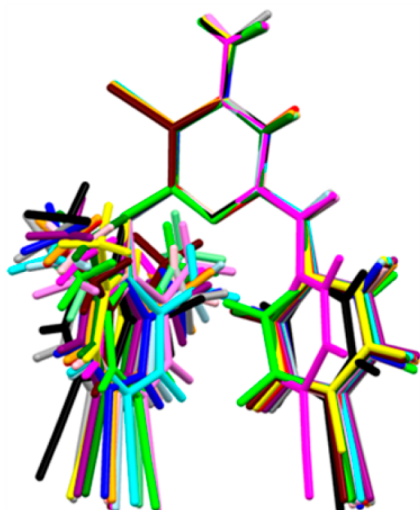


**Figure 9.** Molecular overlay of etravirine. 1: blue, 2: pink, 3: red, 4: orange, 5X: yellow, 5Y: light green, 6: dark green, 7: light blue, 8: cyan, 9: purple, 10: violet, 11X: magenta, 11Y: dark gray, 12X: black, 12Y: brown, and 13: green. (X and Y are the two molecules from the asymmetric unit for a particular compound).

**Conformation of Etravirine.** Etravirine is a conformationally flexible molecule and, in principle, can adopt different conformations in its crystals (Scheme 3). However, in all 13 solid forms, it is observed that the molecule adopts only conformation (A) (i.e., a V-shaped geometry). Molecular overlay (Figure 9) indicates that there is a little torsion in the phenyl rings. This geometry is stabilized by edge-to-face  $\pi\cdots\pi$  interactions between the arm phenyl rings, which is not possible in the other conformations (B, C, or D). Further, the ortho hydrogen of the Ph ring of conformer A is engaged in intramolecular hydrogen bonding with the pyrimidine nitrogen in this robust geometry. Conformations C and D are energetically not favored because the Ar ring has to rotate along the C–O bond to avoid steric repulsion between the Br and two ortho-methyl substitutions on the Ar ring. However, conformation B is energetically favorable, and there is a possibility (so far not realized) of a polymorph for etravirine with this conformation.<sup>10</sup>

During the preparation of the nitrate salt of etravirine, the Br group on the central pyrimidine ring was substituted by a NO<sub>2</sub> group. However, the point to be noticed here is that the molecule adopts the same V-shaped geometry as observed for etravirine in all the solid forms (Figure S2 of the Supporting Information).

**Powder X-ray Diffraction.** Powder X-ray diffraction is a crucial characterization method to know the bulk purity of the sample.<sup>15</sup> Here, the purity of the new solid bulk forms was confirmed by comparing the calculated X-ray patterns with the experimental ones obtained from crystallization or grinding experiments (see the Supporting Information).

**Thermal Analysis.** Differential scanning calorimetry (DSC) measures the exact melting point and/or decomposition temperature for a solid compound. At the same time, it shows phase transitions for polymorphs or dissociation of the multicomponent system at a certain temperature. DSC can be used to measure even a small amount of impurity in the new solid. Etravirine exhibits a melt endotherm at 252 °C, followed by immediate decomposition (exotherm). But, the hydrochloride and mesylate salts showed broad endotherms in the range of 206–220 °C before dissociating into the API. The besylate and tosylate salts showed higher exotherms in the range of 264–271 °C, which is nothing but a direct decomposition without transforming to API. Cocrystal 7 starts melting at 212 °C and decomposes from 235 °C onward. Cocrystal 8 is stable enough at ambient conditions and loses lattice water in the temperature range of 110–140 °C followed by melting onset at 153 °C. This phenomenon is further confirmed by hot stage microscope images (see the Supporting Information). Formic and acetic acid solvates lose the corresponding solvent in the range of 100–140 °C and transform to the API before final decomposition. Acetonitrile solvates lose the solvent comparatively at higher temperature in the range of 160–170 °C and transform to the API before final decomposition, which is further confirmed by hot stage microscope images (see the Supporting Information). Overall, the new solid forms show distinct decomposition pathways.

**Solubility Study.** Solubility is one of the important preformulation properties that has a significant effect on dissolution as well as on the bioavailability of an API. There are several methods to improve the solubility of poorly aqueous soluble APIs; these include formation of nanoparticles, solid dispersions, cyclodextrin complexes, the inclusion of additives (excipients), amorphous phases, cocrystals, and salts.<sup>5</sup> Among these, salt formation is the most commonly used technique in the pharmaceutical industry because of the high solubility and purity of most salts.

There is no report on the solubility study of etravirine in the literature. However, there are reports on formulation of the API as a solid dispersion.<sup>10</sup> The compound is almost insoluble in water over a wide range of pH. Hence, there is a need to improve the solubility which can increase the poor bioavailability of the compound. In search of alternative solid forms with better solubility, salts and cocrystals were prepared. A 50%

**Table 2.** Solubility Profiles of Etravirine and Its New Solid Forms in 50% EtOH at 25 °C

crystalline forms	absorption coefficient (mM <sup>-1</sup> cm <sup>-1</sup> )	apparent solubility (mg/L)		solubility (mg/L)			residue obtained in solubility experiment after		
		1 h	4 h	24 h			1 h	4 h	24 h
1: ETR	41.33	74.3	–	–	–	–	ETR	–	–
2: HETR-Cl	35.73	114.7	–	–	–	–	ETR	–	–
3: HETR-CH <sub>3</sub> SO <sub>3</sub>	59.70	56.6	–	–	–	–	ETR	–	–
5: HETR-C <sub>6</sub> H <sub>5</sub> SO <sub>3</sub>	35.18	118.1	–	–	–	–	ETR	–	–
6: HETR-MeC <sub>6</sub> H <sub>4</sub> SO <sub>3</sub>	48.83	116.6	99.0	–	–	–	ETR + 6	ETR	–
7: ETR-ADP	39.34	118.7	–	–	–	–	ETR	–	–
8: ETR-H <sub>3</sub> BTC-H <sub>2</sub> O	11.37	110.1	396.8	456.0	–	–	8	8	8

EtOH–water solvent mixture was chosen for solubility experiments, as etravirine shows better solubility in 74 mg/L at 1 h of dissolution.<sup>16</sup> The solubility experiments of the solid forms (salts and cocrystals) were carried out in 50% aqueous EtOH, and the phase stability was studied at the interval of 1 h, 4 h, and 24 h. It was observed that in the case of salts and the adipic acid cocrystal (7), the apparent solubility is improved only 1.5 times compared to the parent API, whereas cocrystal 8 shows solubility enhancements up to 5-fold within a 4 h time interval (Table 2). The hydrochloride, mesylate, besylate salts, and cocrystal 7 were found to be less stable and within 1 h were dissociated into the API. However, the tosylate salt is comparatively stable with half (52%) the salt remaining intact after 1 h; complete dissociation was observed after 4 h. Interestingly, cocrystal 8 did not show any change in its powder pattern and was found to be stable even after a 24 h slurry experiment (see the PXRD comparison in the Supporting Information). The difference in the stability of cocrystals is reflected in the calculated density from the single crystal data. Cocrystal 7 has the lowest density (1.434 g/cm<sup>3</sup>) among the solid forms, whereas 8 has the highest (1.572 g/cm<sup>3</sup>), indicating a better packing.

The salt cofomers (hydrochloric acid, methanesulfonic acid, benzenesulfonic acid, and *p*-toluenesulfonic acid) used here are highly soluble/miscible in water and form an incongruent system with the API.<sup>17</sup> Hence, there is a greater probability of dissociation of the salt; this is indeed observed here in the slurry experiment of a 1 h interval. Comparatively speaking, benzenetricarboxylic acid is less soluble and might be forming a better congruent system (less solubility difference between API and cofomer) of comparable solubility in cocrystal 8, which would exhibit better stability even after the 24 h slurry experiment. Among the cocrystals, 7 shows poor stability and, hence, poor solubility. From the structural point of view, 7 exhibits an API:coformer ratio 1:0.5 and involves a strong interaction through synthon II in 1D only. However, 8 exhibits the API:coformer ratio 1:1 and involves a strong interaction in 2D, as well as 3D, due to the inclusion of water, which ultimately improves the stability. Further, in the packing of 7, one molecule of API is surrounded by five API molecules except from the synthon II side; it also has the same 1D chain as seen in the anhydrous form. This arrangement helps to increase the rate of dissociation of the cocrystal to API. In 8, however, there is no direct API–API interaction, and the API is mostly surrounded by H<sub>3</sub>BTC, which helps in improving solubility. In summary, cocrystal 8 shows the best solubility (456 mg/L) among the new multicomponent systems of etravirine isolated in this study.

## CONCLUSIONS

To improve the solubility of etravirine, multicomponent screening was carried out. Thirteen new solid forms of etravirine were obtained in the form of salt, cocrystal, and solvates. Etravirine was found to be capable of forming salts only with the strong acids because of its low basicity. The tendency to form solvates can be attributed to the imbalance of the donor–acceptor ratio within the molecule. Polymorph screening resulted in only one anhydrous form in a different solvent and solvent combinations. A conformational study on etravirine reveals that it can adopt four major possible geometries. However, in all the 13 solid forms, it was found to adopt only one conformation. This can be attributed to the stability provided by the intramolecular edge-to-face  $\pi\cdots\pi$

interaction and the C–H $\cdots$ N hydrogen bond. The strong intermolecular hydrogen bonding involved in etravirine leads to its poor aqueous solubility. The cocrystal approach was found to be a better option for improving the solubility of etravirine compared to salt formation. Cocrystals have shown up to a 6-fold increase in solubility with respect to the parent API, whereas only 1.5 times improvement was shown by salts and that too with poor attendant stability.

## EXPERIMENTAL SECTION

**General Procedures.** Etravirine was obtained from Mylan laboratories, Hyderabad, India. All other reagents were purchased from commercial sources and were used without further purification. Fourier Transform-infrared (FT-IR) spectra were recorded as KBr pellets with a Perkin-Elmer spectrophotometer (4000–400 cm<sup>-1</sup>). Powder X-ray diffraction (PXRD) data were recorded using a Philips X'pert Pro X-ray powder diffractometer equipped with an X'cellerator detector at room temperature with the scan range  $2\theta = 3$  to 40° and step size 0.017°. X'Pert HighScore Plus was used to stack the experimental PXRD pattern with the calculated lines from the crystal structure. DSC was performed on a Mettler Toledo DSC 822<sup>e</sup> module with the heating rate of 5 °C/min between the temperature range of 30–300 °C under nitrogen atmosphere.

**Preparation of Solid Forms.** (1) ETR: crystallized from CHCl<sub>3</sub>. (2) HETR·Cl: Salt 2 was crystallized by dissolving 15 mg of etravirine in 4 mL of a solvent mixture of EtOH:CH<sub>3</sub>NO<sub>2</sub> (1:1) with 4 drops of concentrated HCl. (3) (HETR·CH<sub>3</sub>SO<sub>3</sub>): Salt 3 was crystallized by dissolving 15 mg of etravirine in 4 mL of a solvent mixture of EtOH:CH<sub>3</sub>NO<sub>2</sub> (1:1) with 4 drops of CH<sub>3</sub>SO<sub>3</sub>H. (4) (HETR·H<sub>2</sub>SO<sub>4</sub>·CH<sub>3</sub>OH): Salt 4 was crystallized by dissolving 15 mg of etravirine in 4 mL of a solvent mixture of MeOH:CH<sub>3</sub>NO<sub>2</sub> (1:1) with 4 drops of a concentrated H<sub>2</sub>SO<sub>4</sub>. (5) (HETR·C<sub>6</sub>H<sub>5</sub>SO<sub>3</sub>): 15 mg (0.035 mmol) of etravirine and 11 mg (0.070 mmol) of benzenesulfonic acid were ground together and dissolved in 4 mL of an EtOH:CH<sub>3</sub>NO<sub>2</sub> (1:1) solvent mixture. Block-shaped crystals were obtained within a week. (6) (HETR·MeC<sub>6</sub>H<sub>4</sub>SO<sub>3</sub>): 15 mg (0.035 mmol) of etravirine and 14 mg (0.074 mmol) of *p*-toluenesulfonic acid hydrate were ground together and dissolved in 4 mL of an EtOH:CH<sub>3</sub>NO<sub>2</sub> (1:1) solvent mixture. Block-shaped crystals were crystallized within a week. (7) (2ETR·ADP): 30 mg (0.069 mmol) of etravirine and 6 mg (0.041 mmol) of adipic acid were ground together and dissolved in a minimum amount of CH<sub>3</sub>NO<sub>2</sub> (3 mL). Rectangular block-shaped crystals were crystallized within 3 days. (8) (ETR·H<sub>3</sub>BTC·H<sub>2</sub>O): 15 mg (0.035 mmol) of etravirine and 15 mg (0.071 mmol) of 1,3,5-benzenetricarboxylic acid were ground together and dissolved in 4 mL of MeOH. Block-shaped crystals were obtained in a week. (9) (ETR·HCOOH), compound 9, was crystallized by dissolving 25 mg of etravirine in 5 mL of a solvent mixture of HCOOH:EtOH:CH<sub>3</sub>NO<sub>2</sub> (1:2:2). (10) (ETR·CH<sub>3</sub>COOH), compound 10, was crystallized by dissolving 25 mg of Etravirine in 5 mL of a solvent mixture of CH<sub>3</sub>COOH:EtOH:CH<sub>3</sub>NO<sub>2</sub> (1:2:2). (11) (2ETR·MeOH) and (12), (ETR·MeOH), were crystallized from MeOH and obtained in the same vial as a block- and plate-shaped crystals, respectively. (13) (ETR·CH<sub>3</sub>CN): Crystallized from CH<sub>3</sub>CN.

**Single Crystal X-ray Diffraction.** Except for 13, single crystal X-ray data for all crystals were collected on a Rigaku Mercury 375/M CCD (XtaLAB mini) diffractometer using graphite monochromated Mo K $\alpha$  radiation. The data were processed with Rigaku CrystalClear.<sup>18</sup> For the crystals of 13, the data was collected on a Bruker APEX-II CCD diffractometer using graphite monochromated Mo K $\alpha$  radiation and was processed using SMART (Bruker 2004). Structure solution and refinements were executed using SHELX-97,<sup>19a</sup> using the WinGX<sup>19b</sup> suite of programs. Refinement of coordinates and anisotropic thermal parameters of non-hydrogen atoms were performed with the full-matrix least-squares method. The differing treatment of H atoms in D–H in any structure depends on the data quality. The hydrogen atoms position was located from difference Fourier map or calculated using a riding model. PLATON<sup>20</sup> was used to prepare material for publication, and Material Studio, version 6.0,<sup>21</sup>

was utilized for molecular representations and packing diagrams. Crystallographic cif files (CCDC nos. 933645–933657) are available at [www.ccdc.cam.ac.uk/data\\_request/cif](http://www.ccdc.cam.ac.uk/data_request/cif) or as part of the Supporting Information.

**Solubility Study.** The absorption coefficient of each solid form and API were measured from the slope of the absorbance versus concentration of the five known concentration solutions in a water–EtOH (1:1) solvent mixture. The absorbance was measured at 317 nm to avoid coformer interference (in the 250–280 nm region) on a Perkin-Elmer UV–vis spectrometer. The solubility of each solid was measured at 1 h, 4 h, and 24 h time intervals, using the shake-flask method.<sup>22</sup>

## ■ ASSOCIATED CONTENT

### Supporting Information

Hydrogen bonding parameters, FT-IR, PXRD, and DSC of compounds. This material is available free of charge via the Internet at <http://pubs.acs.org>.

## ■ AUTHOR INFORMATION

### Corresponding Author

\*E-mail: [desiraju@ssc.uisc.ernet.in](mailto:desiraju@ssc.uisc.ernet.in). Fax: +91 80 23602306. Tel: +91 80 22933311.

### Notes

The authors declare no competing financial interest.

## ■ ACKNOWLEDGMENTS

We are thankful to Dr. Ram Jetti (Mylan Laboratories, Hyderabad) for providing the sample of the API. L.R. thanks the DST for a Young Scientist Fellowship. P.S. thanks Ranbaxy Pharmaceuticals for a Fellowship. G.R.D. thanks the DST for a J. C. Bose Fellowship.

## ■ REFERENCES

- (1) (a) Desiraju, G. R. *Crystal Engineering: The Design of Organic Solids*; Elsevier: Amsterdam, 1989; pp 175–198. (b) Desiraju, G. R. *Angew. Chem., Int. Ed.* **1995**, *34*, 2311–2327. (c) *Making Crystals by Design: From Molecules to Molecular Materials, Methods, Techniques, Applications*; Grepioni, F.; Braga, D.; Eds.; Wiley-VCH: Weinheim, Germany, 2007; pp 209–240.
- (2) Generally Regarded as Safe chemicals by the U.S. FDA. <http://www.fda.gov/Food/IngredientsPackagingLabeling/FoodAdditivesIngredients/ucm091048.htm> (accessed March 24, 2013).
- (3) (a) Grant, D. J. W.; Brittain, H. G. Solubility of Pharmaceutical Solids. In *Physical Characterization of Pharmaceutical Solids*; Brittain, H. G., Ed.; Marcel Dekker, Inc.: New York, 1995; pp 321–386. (b) Remenar, J. F.; Morissette, S. L.; Peterson, M. L.; Moulton, B.; Mac-Phee, J. M.; Guzmán, H.; Almarsson, Ö. *J. Am. Chem. Soc.* **2003**, *125*, 8456–8457. (c) Huang, L. F.; Tong, W. Q. *Adv. Drug Delivery Rev.* **2004**, *56*, 321–334. (d) Trask, A. V.; Motherwell, W. D. S.; Jones, W. *Cryst. Growth Des.* **2005**, *5*, 1013–1021. (e) Jones, W.; Motherwell, W. D. S.; Trask, A. V. *MRS Bull.* **2006**, *31*, 875–879. (f) Karki, S.; Friscic, T.; Fabian, L.; Laiti, P. R.; Day, G. M.; Jones, W. *Adv. Mater.* **2009**, *21*, 3905–3909. (g) Schultheiss, N.; Newman, A. *Cryst. Growth Des.* **2009**, *9*, 2950–2967. (h) Brits, M.; Liebenberg, W.; De Villiers, M. M. *J. Pharm. Sci.* **2010**, *99*, 1138–1151. (i) Cheney, M. L.; Shan, N.; Healey, E. R.; Hanna, M.; Wojtas, L.; Zaworotko, M. J.; Sava, V.; Song, S.; Sanchez-Ramos, J. R. *Cryst. Growth Des.* **2010**, *10*, 394–405. (j) Smith, A. J.; Kavuru, P.; Wojtas, L.; Zaworotko, M. J.; Shytle, R. D. *Mol. Pharmaceutics* **2011**, *8*, 1867–1876.
- (4) (a) Thayer, A. M. *Chem. Eng. News* **2007**, *85*, 17–30. (b) Prohotsky, D. L.; Zhao, F. *J. Pharm. Sci.* **2012**, *101*, 1–6.
- (5) (a) Leuner, C.; Dressman, J. *Eur. J. Pharm. Biopharm.* **2000**, *50*, 47–60. (b) Anand, P.; Kunnumakkara, A. B.; Newman, R. A.;

Aggarwal, B. B. *Mol. Pharmaceutics* **2007**, *4*, 807–818. (c) Darwish, M. K.; Foad, M. M. *Drug Discoveries Ther.* **2009**, *3*, 27–36.

(6) (a) McNamara, D. P.; Childs, S. L.; Giordano, J.; Iarriccio, A.; Cassidy, J.; Shet, M. S.; Mannion, R.; O'Donnell, E.; Park, A. *Pharm. Res.* **2006**, *23*, 1888–1897. (b) Good, D. J.; Rodríguez-Hornedo, N. *Cryst. Growth Des.* **2009**, *9*, 2252–2264. (c) Banerjee, R.; Bhatt, P. M.; Ravindra, N. V.; Desiraju, G. R. *Cryst. Growth Des.* **2005**, *5*, 2299–2309. (d) Portell, A.; Barbas, R.; Font-Bardia, M.; Dalmases, P.; Prohens, R.; Puigjaner, C. *CrystEngComm* **2009**, *11*, 791–795. (e) Aitipamula, S.; Wong, A. B. H.; Chowa, P. S.; Tan, R. B. H. *CrystEngComm* **2012**, *14*, 8515–8524.

(7) (a) Bhatt, P. M.; Ravindra, N. V.; Banerjee, R.; Desiraju, G. R. *Chem. Commun. (Cambridge, U.K.)* **2005**, 1073–1075. (b) Trask, A. V.; Motherwell, W. D. S.; Jones, W. *Int. J. Pharm.* **2006**, *320*, 114–123. (c) Aakeröy, C. B.; Forbes, J.; Desper, J. *J. Am. Chem. Soc.* **2009**, *131*, 17048–17049. (d) Bolla, G.; Sanphui, P.; Nangia, A. *Cryst. Growth Des.* **2013**, *13*, 1988–2003.

(8) (a) Bernstein, J. Conformational Polymorphism. In *Organic Solid State Chemistry*; Desiraju, G. R., Ed.; Elsevier: Amsterdam, 1987; pp 471–518. (b) Dunitz, J. D. *Pure and Applied Chemistry* **1991**, *63*, 177–185. (c) Threlfall, T. L. *Analyst* **1995**, *120*, 2435–2460. (d) Desiraju, G. R. *Angew. Chem., Int. Ed.* **2007**, *46*, 8342–8356. (e) Griesser, U. J.; Jetti, R. K. R.; Haddow, M. F.; Brehmer, T.; Apperley, D. C.; King, A.; Harris, R. K. *Cryst. Growth Des.* **2008**, *8*, 44–56. (f) Castro, R. A. E.; Maria, T. M. R.; Evora, A. O. L.; Feiteira, J. C.; Silva, M. R.; Beja, A. M.; Canotilho, J.; Eusbio, M. E. S. *Cryst. Growth Des.* **2010**, *10*, 274–282.

(9) (a) Bhatt, P. M.; Azim, Y.; Thakur, T. S.; Desiraju, G. R. *Cryst. Growth Des.* **2009**, *9*, 951–957. (b) Mahapatra, S.; Thakur, T. S.; Joseph, S.; Varughese, S.; Desiraju, G. R. *Cryst. Growth Des.* **2010**, *10*, 3191–3202.

(10) (a) EMEA/CHMP/43952/2008 Assessment Report for Intelece; European Medicines Agency: London, 2008, [http://www.ema.europa.eu/docs/en\\_GB/document\\_library/EPAR\\_-\\_Public\\_assessment\\_report/human/000900/WC500034183.pdf](http://www.ema.europa.eu/docs/en_GB/document_library/EPAR_-_Public_assessment_report/human/000900/WC500034183.pdf) (accessed June 21, 2013). (b) Scholler-Gyure, M.; Kakuda, T. N.; Raoof, A.; De Smedt, G.; Hoetelmans, R. M. *Clin Pharmacokinet.* **2009**, *48*, 561–574. (c) Sepelj, M.; Leksic, E.; Marinkovic, M.; Krijamancic, I. Polymorphs of Etravirine and Processes for Preparation Thereof. *WOM 2010/131118 A2*, November 2010. (d) Sansone, M. F.; Baert, L. E. C.; Tawa, M.; Remenar, J. F. Co-crystal of Etravirine and Nicotinamide. *US2012028998 A1*, February 2012.

(11) (a) Amidon, G. L.; Lennernas, H.; Shah, V. P.; Crison, J. R. *Pharm. Res.* **1995**, *12*, 413–420. (b) Benet, L. Z.; Amidon, G. L.; Barends, D. M.; Lennernas, H.; Polli, J. E.; Shah, V. P.; Stavchansky, S. A.; Yu, L. X. *Pharm. Res.* **2008**, *52*, 483–488.

(12) (a) Das, K.; Clark, A. D., Jr.; Lewi, P. J.; Heeres, J.; De Jonge, M. R.; Koymans, L. M.; Vinkers, H. M.; Daeyaert, F.; Ludovici, D. W.; Kukla, M. J.; De Corte, B.; Kavash, R. W.; Ho, C. Y.; Ye, H.; Lichtenstein, M. A.; Andries, K.; Pauwels, R.; De Bethune, M. P.; Boyer, P. L.; Clark, P.; Hughes, S. H.; Janssen, P. A.; Arnold, E. *J. Med. Chem.* **2004**, *47*, 2550–2560. (b) Lapadula, G.; Soria, A.; Gori, A. *Clin. Med.: Ther.* **2009**, *1*, 483–494. (c) Lansdon, E. B.; Brendza, K. M.; Hung, M.; Wang, R.; Mukund, S.; Jin, D.; Birkus, G.; Kutty, N.; Liu, X. *J. Med. Chem.* **2010**, *53*, 4295–4299. (d) de Bethune, M.-P. *Antiviral Res.* **2010**, *85*, 75–90. (e) Calin, R.; Paris, L.; Simon, A.; Peytavin, G.; Wiriden, M.; Schneider, L.; Valantin, M.-A.; Tubiana, R.; Agher, R.; Katlama, C. *Antiviral Ther.* **2012**, *17*, 1601–1604. (f) Agneskog, E.; Nowak, P.; Kaellander, C. F. R.; Soennerborg, A. *J. Med. Virol.* **2013**, *85*, 703–708.

(13) Guidance for Industry: Regulatory Classification of Pharmaceutical Co-Crystals; U.S. Department of Health and Human Services, FDA, Center for Drug Evaluation and Research (CDER): Silver Spring, MD, 2013 (<http://www.fda.gov/downloads/Drugs/Guidances/UCM281764.pdf>).

(14) Aitipamula, S.; Banerjee, R.; Bansal, A. K.; Biradha, K.; Cheney, M. L.; Choudhury, A. R.; Desiraju, G. R.; Dikundwar, A. G.; Dubey, R.; Duggirala, N.; Ghogale, P. P.; Ghosh, S.; Goswami, P. K.; Goud, N. R.; Jetti, R. K. R.; Karpinski, P.; Kaushik, P.; Kumar, D.; Kumar, V.;

Moulton, B.; Mukherjee, A.; Mukherjee, G.; Myerson, A. S.; Puri, V.; Ramanan, A.; Rajamannar, T.; Reddy, C. M.; Rodriguez-Hornedo, N.; Rogers, R. D.; Row, T. N. G.; Sanphui, P.; Shan, N.; Shete, G.; Singh, A.; Sun, C. C.; Swift, J. A.; Thaimattam, R.; Thakur, T. S.; Thaper, R. K.; Thomas, S. P.; Tothadi, S.; Vangala, V. R.; Vishweshwar, P.; Weyna, D. R.; Zaworotko, M. J. *Cryst. Growth Des.* **2012**, *12*, 2147–2152.

(15) (a) Remenar, J. F.; Peterson, M. L.; Stephens, P. W.; Zhang, Z.; Zimenkov, Y.; Hickey, M. B. *Mol. Pharmaceutics* **2007**, *4*, 386–400. (b) Karki, S.; Friščić, T.; Fábán, T.; Jones, W. *CrystEngComm* **2010**, *12*, 4038–4041. (c) André, V.; Fernandes, A.; Santos, P. P.; Duarte, M. T. *Cryst. Growth Des.* **2011**, *11*, 2325–2334.

(16) (a) Bauer, J.; Spanton, S.; Henry, R.; Quick, J.; Dziki, W.; Porter, W.; Morris, J. *Pharm. Res.* **2001**, *18*, 859–866. (b) Sanphui, P.; Bolla, G.; Nangia, A. *Cryst. Growth Des.* **2012**, *12*, 2023–2026.

(17) (a) Friščić, T.; Childs, S. L.; Rizvi, S. A. A.; Jones, W. *CrystEngComm* **2009**, *11*, 418–426. (b) Alhalaweh, A.; Velaga, S. P. *Cryst. Growth Des.* **2010**, *10*, 3302–3305. (c) Rodríguez-Hornedo, N.; Nehm, S. J.; Seefeldt, K. F.; Pagán-Torres, Y.; Falkiewicz, C. J. *Mol. Pharmaceutics* **2006**, *3*, 362–367. (d) Goud, N. R.; Gangavaram, S.; Suresh, K.; Pal, S.; Manjunatha, N. G.; Nambiar, S. J. *Pharm. Sci.* **2012**, *101*, 664–680.

(18) Rigaku Mercury375R/M CCD. Crystal Clear-SM Expert 2.0 rc14; Rigaku Corporation: Tokyo, Japan, 2009.

(19) (a) Sheldrick, G. M. *Acta Crystallogr.* **2008**, *A64*, 112–122.

(b) Farrugia, L. J. *J. Appl. Crystallogr.* **1999**, *32*, 837–838.

(20) (a) Spek, A. L. *PLANTON, A Multipurpose Crystallographic Tool*; Utrecht University: Utrecht, The Netherlands, 2002; (b) Spek, A. L. Single crystal structure validation with the program PLATON. *J. Appl. Crystallogr.* **2003**, *36*, 7–13.

(21) Materials Studio, version 6.0; Accelrys Corporation: San Diego, CA, 2011.

(22) Glomme, A.; Marz, J.; Dressman, J. B. *J. Pharm. Sci.* **2005**, *94*, 1–16.